RECONSTRUCTION TECHNIQUE OF FLUORESCENT X-RAY COMPUTED TOMOGRAPHY USING SHEET BEAM

Shunsuke Nakamura, Qingkai Huo, Tetsuya Yuasa

Yamagata University, 4-3-16 Jonan, Yonezawa, Yamagata 992-8510, Japan

ABSTRACT

We clarify the measurement process of fluorescent x-ray computed tomography (FXCT) using sheet-beam as incident beam, and show that the process leads to the attenuated Radon transform. In order to improve quantitativeness, we apply Natterer's scheme to the FXCT reconstruction. We show its efficacy by computer simulation.

Index Terms—Fluorescent x-ray, computed tomography, quantitativeness, reconstruction, attenuated Radon transform

1. INTRODUCTION

The fluorescent x-ray analysis method has been used in tracer non-radioactive element detection studies, with sensitivities reaching one picogram per gram of certain elements [1-4]. In addition, use of synchrotron radiation (SR) as an x-ray source instead of using a conventional x-ray tube remarkably improves the sensitivity. The advantages of SR over an x-ray tube are: 1) high brilliance; 2) broad continuous spectrum; and 3) small beam divergence. From these properties, a thin, parallel, and monochromatic x-ray beam having sufficient intensity can be obtained as incident x-rays. Another advantageous property of SR for fluorescent x-ray analysis is its linear polarization. The polarized nature of SR allows the reduction of the spectral background originating from Compton scattering in the plane of the storage ring by positioning the detector at 90 degrees to beam in the plane of the polarization.

Fluorescent x-ray computed tomography (FXCT), which combines x-ray fluorescence measurements and tomographic reconstruction algorithms, allows the distribution of trace elements within samples to be investigated with high sensitivity and high quantitativeness at high spatial resolution in a non-destructive and non-invasive manner [5-12]. Therefore, FXCT using synchrotron x-ray can be a novel imaging modality for biomedical sciences having both a high spatial resolution and a high sensitivity.

Although FXCT allowed a high spatial resolution, this approach was hampered by the long measurement time required, as conventional FXCT was based on the first generation type of computed tomography (CT), which acquires a set of projections by translational and rotational scans using pencil-beam geometry [13-22]. In order to overcome the difficulties, we proposed the rapid scanning protocol using a linear sensors array with sheet beam [23]. So far, we have proved by *ex-vivo* imaging experiments using synchrotron x-ray that the preliminary FXCT system based on the rapid scanning protocol using sheet incident beam will obtain the information of blood flow in the rat brain with high spatial resolution. However, while we so far used the filtered backprojection (FBP) method as a reconstruction algorithm, the measurement process of FXCT is more complex than the usual CT. Thus, the reconstruction based on the actual measurement process is indispensable for improved quantitativeness. In the present research, we clarify that the measurement process is similar to that of SPECT, and then propose the analytical reconstruction algorithm for FXCT based on that of SPECT devised by Natterer. Finally, we show the effectiveness with computer simulation.

2. IMAGING SYSTEM

For faster measurements, simultaneous or parallel acquisition of a single projection is indispensable. We, therefore, adopted sheet-beam geometry with a linear detectors array [23]. Fig. 1 shows a schematic diagram of the proposed imaging geometry. An incident monochromatic sheet beam generated from synchrotron radiation using a monochromator, where photon fluxes are parallel to one another and are linearly polarized in a plane containing the cross-section of interest, impinges on the object to cover the width of the object cross-section. Imaging agents, such as iodine, are thus excited and isotropically emit x-ray fluorescence photons on de-excitation. A linear array of detectors, where N solid state detectors operating in a photon-counting mode with energy resolution are equally spaced, is positioned perpendicular to the beam propagation direction in the plane of polarization. Due to the property of linear polarization the emission of Compton scattered photons is lowest. The net counts in the characteristic X-ray fluorescent spectral lines at each projection point constitute the CT projections. The energy of the incident beam is carefully tuned so that the fluorescent spectral line does not overlap with the Compton scatter peak.

A long slit-like collimator is installed in front of each detector element in order to restrict the regions emitting x-ray fluorescence incident to the detective surface and to reduce the amount of stray radiation being detected. For example, a detector of interest in Fig. 1 ideally detects just the fluorescent photons on a line perpendicular to the detective surface. Projections are acquired at constant angular steps using a rotation motion of the object over 180. Note that no translational scans are required in the sheet-beam geometry.

To perform attenuation correction, the distributions of the linear attenuation coefficients of the object at the energies of the incident and fluorescent x-rays must be obtained. This information is acquired using a conventional transmission computed tomography setup. This includes positioning of a zero-degree CCD detector in the imaging system (Fig. 1) to measure the transmission CT signal. Two measurements of transmission CT projections are carried out, once at the energy of the incident beam for fluorescent CT, which is measured simultaneously with the FXCT measurement, and once at the energy of the fluorescent spectral line, which is measured separately.

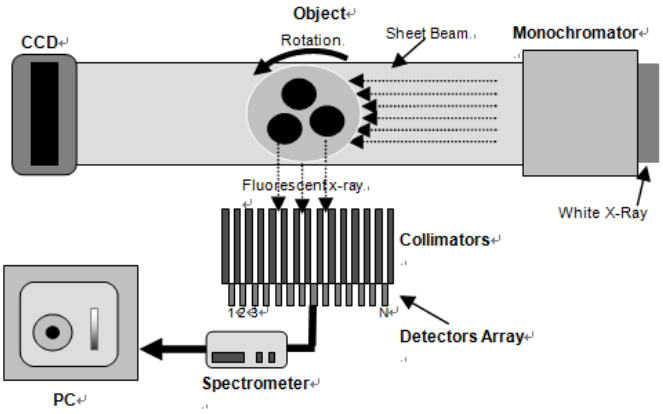

Fig. 1. Schematic diagram of a typical FXCT experimental system based on sheet-beam geometry.

3. FORMULATION OF THE MEASUREMENT PROCESS

We set the x_1x_2-coordinate fixed to the object, and suppose that the sheet beam accompanied with the detectors array is rotated around the origin O, where the collimators in front of the array are omitted so as to see easily the diagram. The hatched region means the incident sheet-beam irradiation.

We derive the formula representing fluorescent x-ray photons measured by a single detector, or the *i*th detector among *N* detectors of the array. First, we pay attention to a single incident ray among the sheet beam. The points, P, Q, S and R in Fig. 2 represent the intersection of the single incident ray with the object's surface, the point of interest, an intersection of a single emitted fluorescent x-ray with the object's surface, and an intersection of line QS with the object's surface, respectively. We denote the iodine concentration distribution to be estimated, the distribution of the linear attenuation coefficient for the energy of the incident X-ray, and that of the fluorescent X-ray as $d(x)$, $a_I(x)$ and $a_F(x)$, respectively. These are two-dimensional (2-D) functions with compact supports, where $x \in \mathbb{R}^2$. $a_I(x)$ and $a_F(x)$ must be known in advance by the usual x-ray CT using the CCD camera shown in Fig. 1.

Next, let us consider the process in which a single incident ray with an initial intensity I_0, at the point, P, arrives at the point, Q, and the fluorescent subsequently emitted x-ray from the iodine atoms excited at the point, Q, reaches the *i*th detector. We partitioned the process into three steps. Here, $\theta \in S^1$ and $\theta^{\perp} \in S^1$ are unit vectors parallel and vertical to the single ray of interest, where S^1 is a unit circle.

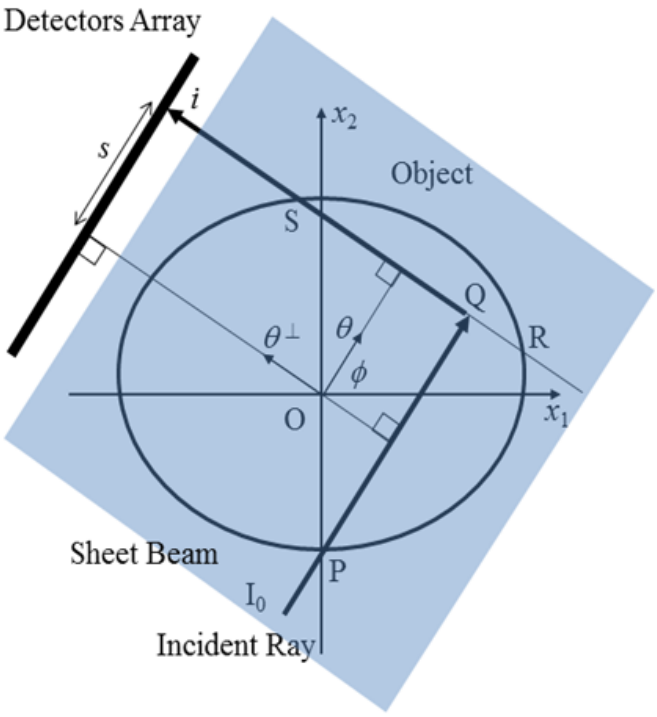

Fig. 2. Schematic diagram of the measurement process

Step *1* (Attenuation of incident x ray): The incident x-ray flux rate, $I(x)$, reaching the point, Q, is given by

$$I(x) = I_0 \mathrm{e}^{-(Da_I)(x,\theta)} \quad , \tag{1}$$

where

$$(Da_I)(x,\theta) = \int_0^{\infty} a_I(x - t\theta)dt \ . \tag{2}$$

Step 2 (Generation of fluorescent x ray): The fluorescent x-ray is emitted isotropically with an intensity proportional to the product of the absorbed x-ray flux rate at the point, Q, $\mu_{ph}\, I(x)\, \Delta v$, and the iodine concentration, $d(x)$, where μ_{ph} is the photoelectric linear attenuation coefficient of iodine, and Δv is the differential volume at Q. Accordingly, the flux rate of the fluorescent x-ray emitted from the point, Q, and reaching the ith detector, $f(x)$, is given by

$$f(x) = I(x)\, d(x)\, \mu_{ph}\, \omega\, \Delta v\, \Omega/4\pi \qquad (3)$$

where ω and Ω are the yield of the fluorescent x-ray and the solid angle at which the point, Q, is viewed by the ith detector, respectively.

Step 3 (Attenuation of fluorescent x ray): Following a fluorescent x-ray emitted from the point, Q, crossing the object toward the ith detector, it is attenuated along the line segment QS; it reaches the ith detector with a flux rate given by

$$I_d(x) = \mathrm{e}^{-(Da_F)\left(x,\theta^{\perp}\right)} f(x)\,, \qquad (4)$$

where

$$(Da_F)(x,\theta^{\perp}) = \int_0^{\infty} a_F\left(x + t\theta^{\perp}\right) dt\,. \qquad (5)$$

Here, we obtained the contribution from the single incident ray into the ith detector. The formula holds for other rays among the sheet beam. The total flux rate of the fluorescent x-ray reaching the ith detector for the sheet beam x-ray is obtained by integrating with respect to x along line RS, $x \cdot \theta = s$, where s is a distance between origin O and line RS:

$$(R_a f)(\theta, s) = \int_{x\cdot\theta=s} \mathrm{e}^{-(Da_F)\left(x,\theta^{\perp}\right)} f(x)\, dx\,. \qquad (6)$$

Thus, the measurement process by the FXCT based on sheet beam geometry leads to the attenuated Radon transform [24].

The inversion for $g = R_a f$ was given by Natterer as

$$f(x) = \frac{1}{4\pi}\mathrm{Re\ div} \int_{S^1} \theta \mathrm{e}^{(Da_F)(x,\theta^{\perp})} (\mathrm{e}^{-h} H\, \mathrm{e}^{h} g)(\theta, x\cdot\theta)\, d\theta\,, \qquad (7)$$

where $h = \frac{1}{2}(I + \mathrm{i}H) R a_F$, and H and R are the Hilbert transform and Radon transform, respectively [24]. We can obtain the exact iodine density $d(x)$ by first applying the exact inversion formula straightforwardly to Eq. (6), and then by applying Eq. (3) to the resulting $f(x)$.

4. SIMULATION

Fig. 3 (a) shows the 256×256 Shepp-Logan phantom used in the simulation. The phantom's dimensions were designed to simulate a mouse head, where the major axis was 40 mm.

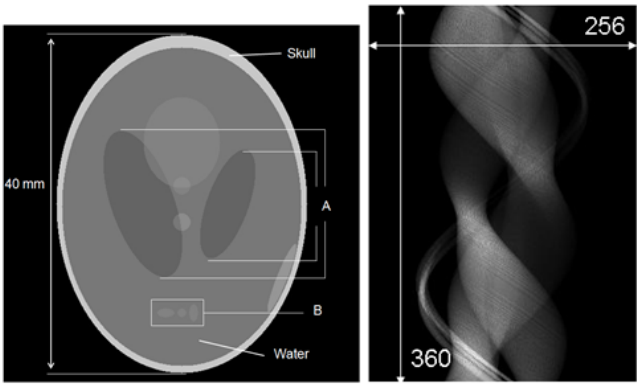

(a) (b)

Fig. 3. (a) Numerical phantom and (b) the sinogram calculated from the phantom.

Energy of the monochromatic incident x-ray beam was set to 37 keV, which is a typical value in the actual experiments. Incident x-ray flux was 9.7×10^7 photons/mm^2/s , with a sheet beam cross section 0.19×0.19 mm^2. The detector slit-like collimater was 0.19 mm wide, 0.19 mm high, and 10 mm deep. The distance between the center of object and entrance to the collimator in front of the central detector was 35 mm. We regarded the skull region shown in Fig. 4 as that consisting of calcium, where the the linear attenuation coefficients of calcium for the incident beam energy (37 keV) and the fluorescent one (28.3 keV) were set to 0.3005 cm^{-1} and 0.4464 cm^{-1}, respectively. Next, we set two kinds of iodine accumulation regions, A and B. The iodine concentration of A and B regions were 80 μg/ml and 160 μg/ml, respectively; The photoelectric linear attenuation coefficient of iodine, μ_{ph}, and the yield of the fluorescent x-ray, ω, were 0.2745 cm^2/g and 0.8, respectively. The other region in the brain was regarded as water. The linear attenuation coefficients of water for the incident beam energy (37 keV) and the fluorescent one (28.3 keV) were set to 0.3005 cm^{-1} and 0.3005 cm^{-1}, respectively. Since the iodine solution was dilute, the attenuation coefficient in the portion including the iodine solution was set to the same value as that of water. We generated 360 projections for the numerical sample according to Eq. (6), with a rotational step of 1 degree over 360 degrees (Fig. 3 (b)).

5. RESULTS

CT images were reconstructed using the proposed method, combined with a filtered back projection (FBP) method with the Shepp-Logan filter without attenuation correction. We show the reconstructed images in Fig. 4. Both routines satisfactorily reconstruct A and B regions. In terms of morphology, there is no difference between the two.

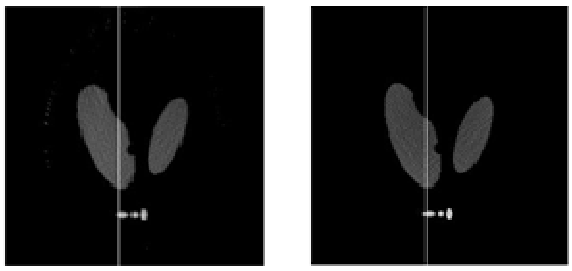

(a) (b)

Fig. 4. Reconstructed images by (a) the proposed method, and (b) the FBP method.

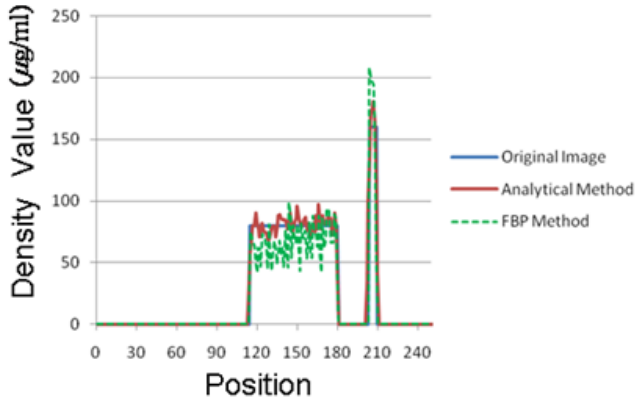

Fig. 5. Line profiles on the line drawn in Figs. 4.

	A Region (μg/ml)	B Region (μg/ml)
Original Image	80	160
Proposed Method	79.8 (9.8)	164.3 (10.3)
FBP Method	67.8 (18.7)	197.4 (24.3)

Table 1. Comparison between the proposed and the FBP methods in quantitativeness.

Next, we compared them in quantitativeness. Fig. 4 compares the original values and the profiles on the lines drawn in Figs. 3 (a) and (b). From the figure, the proposed method is better in both A and B regions than the FBP method, while the both have oscillating components in the regions of interest. In addition, we compared the average values and the standard deviations in A and B regions (Table 1). In the both ROIs, the proposed method is better than the FBP method.

6. SUMMARY

We first introduced an FXCT imaging method using the sheet beam geometry to obtain 2-D tomographic image at high speed, and then considered the forward problem of FXCT using sheet beam geometry. In addition, we proposed an analytical reconstruction method with the help of Natterer's result with respect to attenuated Radon transform, and demonstrated its efficacy by applying the proposed method to synthetic data and comparing the reconstruction result with that by the conventional FBP method.

7. REFERENCES

[1] A. Iida, Y. Gohshi, "Tracer element analysis by X-ray fluorescent," Edited by Ebashi S, Koch M, Rubenstein E, Handbook on Synchrotron Radiation 4, pp. 307-348, North-Holland 1991 Amsterdam, New York, Tokyo.

[2] P. Boisseau, L. Grodzins, "Fluorescence Tomography Using Synchrotron Radiation at the NSLS," Hyperfine Interactions Vol. 33, pp. 283-292, 1987.

[3] R. Cesareo, S. Mascarenhas, "A new tomographic device based on the detection of fluorescent x-rays," NIM A 277, pp. 669-672, 1989.

[4] D.V. Rao, M. Swapna, R. Cesareo, A. Brunetti, T. Akatsuka, T. Yuasa, T. Takeda, G. Tromba and G.E. Gigante, "Synchrotron-induced X-ray fluorescence from rat bone and lumber vertebra of different age groups," NIMB, Vol. 267, Iss. 3, pp. 502-505, 2009.

[5] J.P. Hogan, R.A. Gonsalves, A.S. Krieger, "Fluoresecent computer tomobraphy – A model for correction of x-ray absorption, IEEE Transactions on Nuclear Science," Vol. 38, pp. 1721-1727, 1991.

[6] G.F. Rust, J. Weigelt, "X-ray fluorescent computer tomography with synchrotron radiation," IEEE Transactions on Nuclear Science, Vol. 45, Iss. 1, pp. 75-88, 1998.

[7] A. Simionovici, M. Chukalina, C. Schroer, M. Drakopoulos, A. Snigirev, I. Snigireva, B. Lengeler, K. Janssens, F. Adams, "High-resolution X-ray fluorescence microtomography of homogeneous samples IEEE Transactions on Nuclear Science," Vol. 47, Iss. 6, pp. 2736- 2740, 2000.

[8] C.G. Schroer, "Reconstructing x-ray fluorescence microtomograms," Appl. Phys. Lett., Vol. 79, Iss. 12, pp. 1912-1914, 2001.

[9] B. Golosio, A. Simionovici, A. Somogyi, L. LemelleLemelle L, M. Chukalina, Brunetti, "Internal elemental microanalysis combining x-ray fluorescence, Compton and transmission tomography," J. Appl. Phys., Vol. 94, Iss. 1, pp. 145 -156, 2003.

[10] P.J. La Riviere, P.A. Vargas, "Monotonic penalized-likelihood image reconstruction for X-ray fluorescence computed tomography," IEEE Transactions on Medical Imaging, Vol. 25, Iss. 9, pp. 1117-1129, 2006.

[11] A. Simionovici, M. Chukaline, F. Gunzler, C. Schroer, A. Snigirev, I. Snigireva, J. Tummler, T. Weitkamp, "X-ray microtome by fluorescent tomography," NIMA Vol. 467-468, pp. 889-892, 2001.

[12] B. Menz, A. Simoinovici, P. Philippot, S. Bohic, F. Gibert, M. Chukalina, "X-ray fluorescence micro-tomography of an individual fluid inclusion using a third generation synchrotron light source," NIMB Vol. 181, pp. 749-754, 2002.

[13] T. Takeda, T. Maeda, T. Yuasa, T. Akatsuka, T. Ito, K. Kishi, J. Wu, M. Kazama, K. Hyodo, and Y. Itai: Fluorescent Scanning X-Ray Tomography with Synchrotron Radiation, Review of Scientific Instruments, Vol. 66, No. 2, pp. 1471-1473, 1995.

[14] T. Yuasa, M. Akiba, T. Takeda, M. Kazama, A. Hoshino, Y. Watanabe, K. Hyodo, F.A. Dilmanian, T. Akatsuka, and Y. Itai, "Reconstruction Method for Fluorescent X-Ray Computed Tomography by Least Squares Method Using Singular Value Decomposition," IEEE Transactions on Nuclear Science, Vol. 44, No. 1, pp. 54-62, 1997.

[15] T. Takeda, M. Kazama, T. Zeniya, T. Yuasa, M. Akiba, A. Uchida, K. Hyodo, T. Akatsuka, M. Ando, and Y. Itai, "Development of a Monochromatic X-Ray Computed Tomography with Synchrotron Radiation for Functional Imaging," in Medical Applications of Synchrotron Radiation, (Springer-Verlag, Tokyo), pp. 103-110, 1998.

[16] T. Takeda, A. Momose, Q. Yu, T. Yuasa, F.A. Dilmanian, T. Akatsuka, and Y. Itai, "New Types of X-Ray Computed Tomography with Synchrotron Radiation: Fluorescent X-Ray CT and Phase Contrast X-

Ray CT Using Interferometer," Cellular and Molecular Biology, Vol. 46, No. 6, pp. 1077-1088, 2000.
[17] Q. Yu, T. Takeda, T. Yuasa, Y. Hasegawa, J. Wu, Thet-Thet-Lwin, K. Hyodo, F.A. Dilmanian, Y. Itai, and T. Akatsuka, "Preliminary Experiment of Fluorescent X-Ray Computed Tomography to Detect Dual Agents for Biological Study," Journal of Synchrotron Radiation, Vol. 8, pp. 1030-1034, 2001.
[18] T. Takeda, Q. Yu, T. Yashiro, T. Zeniya, J. Wu, Y. Hasegawa, Thet-Thet-Lwin, K. Hyodo, T. Yuasa, F.A. Dilmanian, T. Akatsuka, and Y. Itai, "Iodine Imaging in Thyroid by Fluorescent X-Ray CT with 0.05 mm Spatial Resolution," Nucl. Instrum. Meth. A Vol. 467-468, pp. 1318-1321, 2001.
[19] T. Takeda, "Phase-contrast and fluorescent X-ray imaging for bio-medical researches," Nucl. Instrum. Meth. A 548, pp. 38-46, 2005.
[20] Thet-Thet-Lwin, T. Takeda, J. Wu, N. Sunaguchi, T. Murakami, S. Mouri, S. Nasukawa, Q. Huo, T. Yuasa, K. Hyodo, T. Akatsuka, "Myocardinal Fatty Acid Metabolic Imaging by Fluorescent X-Ray Computed Tomography Imaging," Journal of Synchrotron Radiation, Vol. 14, No. 1, pp. 158-162, 2007.
[21] Thet-Thet-Lwin, T. Takeda, J. Wu, Q. Huo, T. Yuasa, K. Hyodo, and T. Akatsuka, "Visualization of age-dependent cardiomyopathic model hamster obtained by fluorescent X-ray computed tomography using I127-IMP," Journal of. Synchrotron Radiation, Vol. 15, Part 5, pp. 528-531, 2008.
[22] T. Takeda, J. Wu, Thet-Thet-Lwin, Q. Huo, T. Yuasa, K. Hyodo, F.A. Dilmanian, T. Akatsuka, "X-ray fluorescent CT imaging of cerebral uptake of stable-iodine perfusion agent iodoamphetamine analog IMP in mice," Journal of Synchrotron Radiation, Vol. 16, Part 1, pp. 57-62, 2009.
[23] Q. Huo, T. Yuasa, T. Akatsuka, T. Takeda, J. Wu, Thet-Thet-Lwin, K. Hyodo, F.A. Dilmanian, "Sheet-beam geometry for in vivo fluorescent x-ray computed tomography: proof-of-concept experiment in molecular imaging," Optics Letters, Vol. 33, Iss. 21, pp. 2494-2496, 2008.
[24] F. Natterer, "Inversion of the attenuated Radon transform," *Inverse Problems* (17), pp. 112-119, 2009.